Observed Diurnal Cycle Change of Tropical Deep Convection Amplifies Surface Warming

Jakob Deutloff

jakob.deutloff@uni-hamburg.de

Universität Hamburg https://orcid.org/0000-0003-1995-3744

Stefan Buehler

Universität Hamburg https://orcid.org/0000-0001-6389-1160

Julia Windmiller

Monash University

Ann Kristin Naumann

Ludwig-Maximilians-University in Munich https://orcid.org/0000-0002-5057-6038

Article

Keywords: High-Cloud Feedback, Diurnal Cycle, Deep Convection, Climate Sensitivity

Posted Date: April 9th, 2026

DOI: https://doi.org/10.21203/rs.3.rs-9293749/v1

Additional Declarations: There is **NO** Competing Interest.

Observed Diurnal Cycle Change of Tropical Deep Convection Amplifies Surface Warming

Jakob Deutloff[1, 2, 3*], Stefan A. Buehler[1, 2], Julia Windmiller[4], Ann Kristin Naumann[5]

[1*]Earth System Sciences, Atmospheric Science, University of Hamburg, Hamburg, Germany.
[2]Earth and Society Research Hub (ESRAH), Hamburg, Germany.
[3]International Max Planck Research School on Earth System Modelling (IMPRS-ESM), Hamburg, Germany.
[4]Monash University, Melbourne, Australia.
[5]Ludwig-Maximilians-Universität in Munich, Munich, Germany.

*Corresponding author(s). E-mail(s): jakob.deutloff@uni-hamburg.de;
Contributing authors: stefan.buehler@uni-hamburg.de; julia.windmiller@monash.edu; a.naumann@lmu.de;

Abstract

Climate feedbacks from changes in the diurnal cycle of clouds have received limited attention. However, recent storm-resolving aquaplanet simulations predict a partial shift of tropical deep convection from daytime to nighttime in response to surface warming, producing a positive feedback of similar magnitude as other cloud feedbacks. Here, we use satellite observations of ice water path to test whether such a feedback exists. We use the internal variability within 24 years of observations to regress the diurnal cycle of cloud fraction against surface temperature. We find that clouds produced by deep convection partly shift from daytime to nighttime with increasing surface temperature, over both land and ocean. This increases the amount of solar radiation absorbed by the surface and hence constitutes a positive climate feedback. We derive a global feedback value of $\mathbf{0.12 \pm 0.02}$ **W m**$^{\mathbf{-2}}$ **K**$^{\mathbf{-1}}$ for this diurnal-cycle feedback, which adds to previous estimates of the cloud feedback, implying a higher climate sensitivity.

Keywords: High-Cloud Feedback, Diurnal Cycle, Deep Convection, Climate Sensitivity

1 Introduction

Understanding how clouds will amplify or dampen global warming remains a key challenge for narrowing down uncertainty in climate sensitivity. Among all climate feedbacks, the cloud feedback is most uncertain [1], which has motivated numerous studies on this aspect of climate change [2–6]. However, those studies do not include changes in the diurnal cycle of clouds, despite their potential to create a substantial feedback [7, 8]. If clouds shift from daytime to nighttime (or vice versa), this will decrease (increase) the amount of reflected solar radiation and hence amplify (dampen) surface warming.

One reason for the lack of studies targeting the feedback from changes in the diurnal cycle of clouds might be that the conventional framework for analysing the cloud feedback does not account for it. The typical decomposition of the cloud feedback only takes changes in mean cloud quantities into account, like altitude, optical depth or cloud amount [1, 2]. This decomposition is usually done with cloud radiative kernels, which allow for separating changes in cloud properties from changes in the clear-sky atmosphere [9, 10]. However, cloud radiative kernels assume that clouds do not have a diurnal cycle. This makes it impossible to use them for detecting a feedback from changes in the diurnal cycle of clouds.

Another reason why changes in the diurnal cycle of clouds have received limited attention may be that suitable models for studying them only became available recently. The widely used Global Circulation Models (GCMs) are not ready for this task, since they rely on parameterisations of convection, which produce an unrealistic diurnal cycle [11, 12]. This limitation was overcome recently by the development of Global Storm-Resolving Models (GSRMs) that resolve convection explicitly, which leads to a correct representation of the diurnal cycle of convection [13–15].

Recent aquaplanet simulations with a GSRM predict that some of the tropical clouds produced by deep convection shift from daytime to nighttime in response to surface warming, which produces a positive feedback in these simulations [16]. The shift from daytime to nighttime is greatest for the thickest clouds with an ice water path (I) of $I \geq 1$ kgm^{-2}, referred to as deep convective clouds, but also affects thick anvil clouds with 1 kgm$^{-2} > I \geq 0.1$ kgm^{-2}. The resulting feedback diagnosed from the GSRM simulations scaled to a global value is 0.1 W m^{-2} K^{-1} for a uniform surface warming of 2 K and 0.05 W m^{-2} K^{-1} for a 4 K warming. This would enhance the total cloud feedback of 0.45 ± 0.33 W m^{-2} K^{-1} [2] by ten to twenty percent.

The change in the diurnal cycle of deep convection found in the aquaplanet simulations needs to be tested with observations to assess its realism and whether it also applies over land. The diurnal cycle of deep convection is more pronounced over land, where surface heating produces a strong afternoon peak of deep convection, whereas deep convection over the ocean peaks in the early morning hours due to enhanced radiative cooling of the atmosphere at nighttime [17–19].

In this study, we use internal variability within satellite observations of I and two-meter temperature to test whether the positive feedback from changes in the diurnal cycle of tropical deep convection exists in the real world. We find that this is the case, with a partial shift of the deep convection from daytime to nighttime in response to surface warming. This is true over land and ocean, despite large land-ocean differences in the mean diurnal cycle. The change in the diurnal cycle of tropical deep convection and the resulting feedback is stronger in the observations than in the aquaplanet simulations.

2 Identifying Clouds Produced by Deep Convection

We use I as a measure for cloud thickness to distinguish different types of tropical high clouds. This I-perspective has proven to be a valuable framework for analysing the high-cloud feedback [16, 20–22]. We define deep convective clouds as $I > 1$ kg m^{-2} in agreement with earlier studies [16, 23]. While deep convective clouds have the closest link to deep convection, thick anvil clouds detrained from them might also feel changes in the diurnal cycle of deep convection and contribute to the total feedback. Therefore, we include all clouds with $I > 0.1$ kg m^{-2} in our feedback estimate (Sec. 5).

Our analysis is based on the Chalmers Cloud Ice Climatology (CCIC) [24, 25], which uses machine learning to retrieve I from brightness temperature (T_b) measurements. The CCIC dataset has a horizontal grid spacing of 0.036°, a 30 minute timestep and is available for the 2000 to 2024 period. We cannot use direct satellite observations of I, since they are only available from sun-synchronous satellites [26, 27], and hence do not capture the diurnal cycle. To test the robustness of our results, we also use the T_b measurements [28, 29] CCIC is based on to assess changes in the diurnal cycle of deep convective clouds. We constrain our analysis to the tropics (30°S to 30°N).

We establish comparability between measurements of I and T_b by making use of the fact that clouds with the highest I usually also have the coldest T_b. To derive thresholds in T_b that correspond to the I

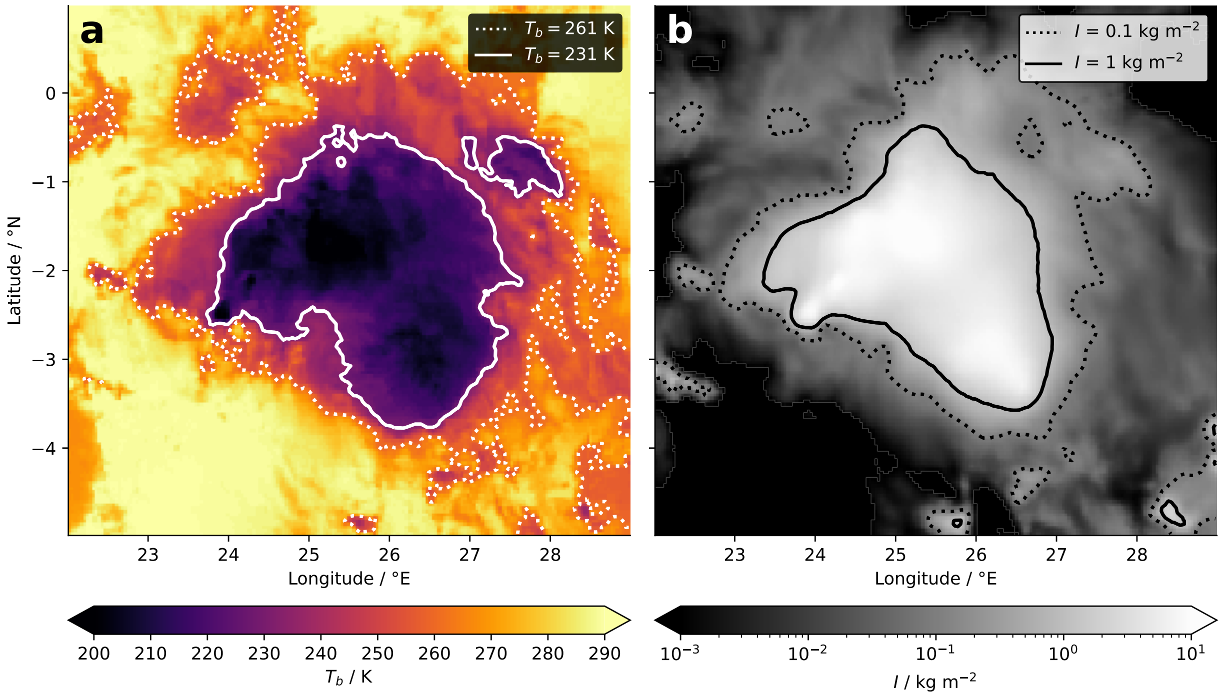

Fig. 1 Brightness temperature T_b and corresponding ice water path I of a mesoscale convective system. Contour lines mark the threshold for deep convective clouds (solid) and thick anvils (dashed).

thresholds, we require the area (A) covered by clouds thicker than a given I_0 to match the area covered by clouds colder than the corresponding $T_{\mathrm{b},0}$:

$$A(I > I_0) = A(T_\mathrm{b} < T_{\mathrm{b},0}). \tag{1}$$

This yields a near-linear relationship of T_b and $\log_{10} I$ (Fig. S1) and suggests $T_\mathrm{b} < 231$ K for deep convective clouds and $T_\mathrm{b} < 261$ K for all clouds contributing to the feedback.

For an example mesoscale convective system, similar clouds are identified as deep convective clouds regardless of whether T_b or I are used (Fig. 1). The cloud area identified via T_b is slightly larger than the cloud area from I. This is possible because the area constraint in Eq. 1 used to derive the relationship of T_b and I is required to hold on average over the whole observation period, and will not hold for every individual scene. The cloud field appears smoother in I than in T_b. This is a consequence of the machine learning algorithm using the spatial structure of T_b to infer I, which causes the effective resolution of I to be lower than the resolution of T_b [24].

3 Diurnal Cycle of Deep Convection

We use the cloud fraction of deep convective clouds (f_d) to analyse the diurnal cycle of deep convection. To this end, we calculate f_d as a function of local time for areas over land, ocean, and the whole tropics by applying the I threshold defined for deep convective clouds (See Methods). The total area fraction covered by deep convective clouds can be derived by summing up f_d over local time, which yields 0.040 over land and 0.032 over ocean.

As expected [30], the diurnal cycle of deep convection is much stronger over land than over ocean (Fig. 2). While deep convection over land has a pronounced peak at 17:30 local time, deep convection over ocean peaks at 5:30 and 14:30. The strong afternoon peak of convection over land is known to be driven by solar surface heating. [31, 32]. Absorbed solar radiation is causing surface temperatures to increase throughout the day, building up atmospheric instability that is consumed by convection in the late afternoon. Since the variability of surface temperature is smaller over ocean than over land, the diurnal cycle is less pronounced and mostly driven by radiative fluxes [17, 19].

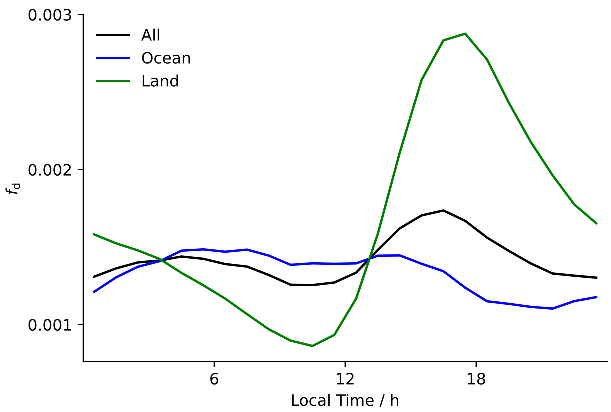

Fig. 2 Mean deep convective cloud fraction (f_d) plotted against local time for the entire tropics (All) and for deep convective clouds over land and ocean.

4 Reduction of Daytime Deep Convection

We assess the change in f_d in response to surface warming by regressing detrended and deseasonalized timeseries of f_d against the corresponding two-meter temperature (T) from ERA5 [33]. We normalise f_d at each timestep to exclude changes that are uniform across the day. Therefore, changes in f_d only account for a shift of the diurnal cycle and add up to zero (see Methods).

Deep convective clouds occur less during the day and more during the night in response to surface warming, confirming the result from GSRM aquaplanet experiments [16] (Fig. 3a). This finding is robust, regardless of whether I or T_b are used to identify deep convective clouds. While the response of the diurnal cycle of f_d is similar in the GSRM and observations, the signal is larger in the observations. In the GSRM, the maximum decrease of f_d is -1.7 % K^{-1} at 13:30 local time, while it is -3.5 % K^{-1} at 13:30 for the I estimate and -5 % K^{-1} at 15:30 for the T_b estimate. One possible reason for the more pronounced change in the diurnal cycle diagnosed from T_b compared to the change diagnosed from I is the lower effective resolution of I (Sec. 2).

Changes in the diurnal cycle of deep convective clouds arise because the response of f_d to surface warming depends on local time. This becomes clear when we do not normalise f_d before regressing it against T, which reveals that deep convective clouds overall decrease, but more so during the day (Fig. S2). The overall decrease and the change in the diurnal cycle are of similar magnitude. Previous studies focusing on the change in high cloud amount, which includes deep convective clouds, missed the diurnal-cycle feedback since

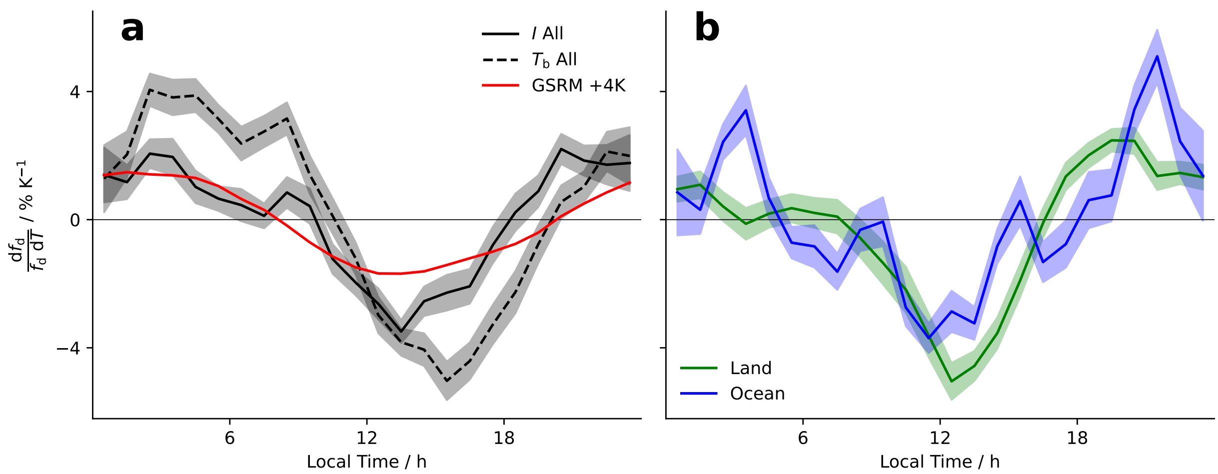

Fig. 3 (**a**) Change of the diurnal cycle of deep convective cloud fraction (f_d) with two-meter temperature T in the tropics diagnosed from brightness temperatures (T_b) and ice water path (I) and from 4 K warming run of the GSRM aquaplanet simulations [16]. (**b**) Change of the diurnal cycle of f_d with T partitioned into land and ocean areas diagnosed from I. Shading marks the standard error of the linear regression.

they only diagnosed the overall change in high cloud amount, and not how this decrease varies across the day [4, 20, 34, 35].

The change in the diurnal cycle of deep convective clouds in response to surface warming is similar over land and ocean (Fig. 3b). This similarity is surprising, given the vast differences in the mean diurnal cycle (Fig. 2) and points towards a shared driving mechanism that is independent of the surface type. It was speculated that a higher magnitude of cloud radiative heating in response to surface warming might drive the change in the diurnal cycle of deep convection [16], but tailored mechanism-denial simulations will be necessary to test this hypothesis.

5 Positive Diurnal-Cycle Feedback

Changes in the diurnal cycle of clouds only affect the shortwave part of the radiative balance, not the longwave part. The incoming shortwave radiation at the top of the atmosphere has a strong diurnal cycle, while the upwelling longwave radiation in clear-sky regions is almost constant in comparison (Fig. S3). Therefore, it is crucial at which local time a cloud occurs for the shortwave part of the radiative balance, while it is negligible for the longwave part. If clouds shift from daytime to nighttime in response to surface warming, more solar radiation is absorbed by the surface, which amplifies surface warming (Fig. 4).

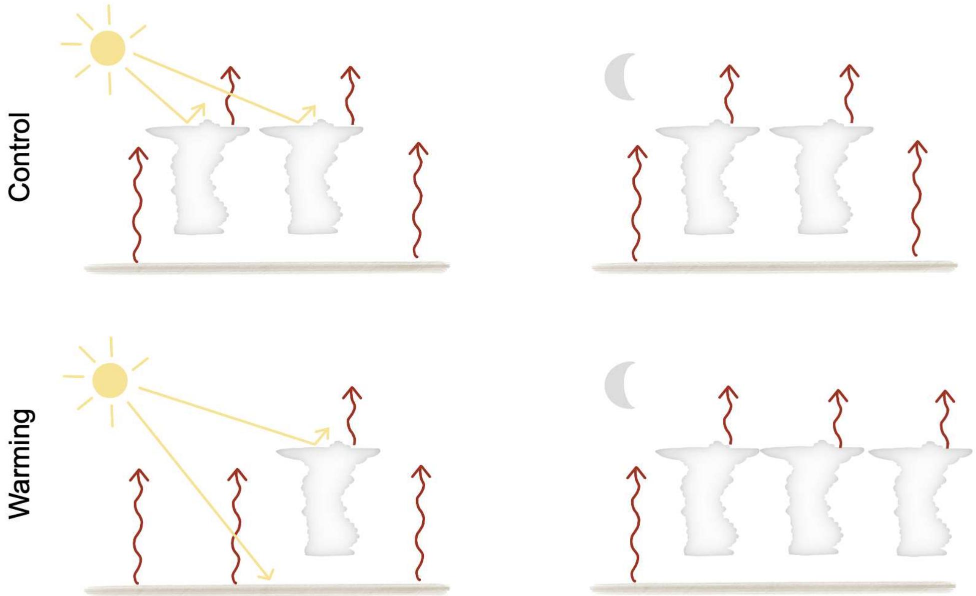

Fig. 4 Schematic of the diurnal-cycle feedback. Red arrows represent the longwave radiative flux, yellow arrows represent the shortwave radiative flux. The upper row shows the control climate, while the bottom row shows a warmer climate.

To estimate the feedback from a reduction of daytime deep convection, we resolve cloud fraction f by cloud thickness measured by I to analyse how clouds with different thicknesses contribute to the total feedback. We include all clouds with $I > 0.1$ kg m^{-2} in our feedback estimate. Thinner clouds within this range might not be directly produced by deep convection, but still feel changes in the diurnal cycle of deep convection. As clouds become thinner than $I = 0.1$ kg m^{-2}, their albedo drops significantly (Fig. S4), hence they will not substantially contribute to the feedback.

We estimate the diurnal-cycle feedback (λ) by calculating the change in reflected solar radiation (R) caused by a change in the diurnal cycle of f. To this end, we approximate R as

$$R(l, I) = S(l) \cdot \alpha_{\mathrm{cl}}(l, I) \cdot f(l, I) + S(l) \cdot \alpha_{\mathrm{cs}} \cdot [1 - f(l, I)], \quad (2)$$

where α_{cl} is the cloud albedo, α_{cs} is the clear-sky albedo, S is the incoming solar radiation and l local time. The diurnal-cycle feedback λ is calculated as the change in R with T due to changes in the diurnal cycle of

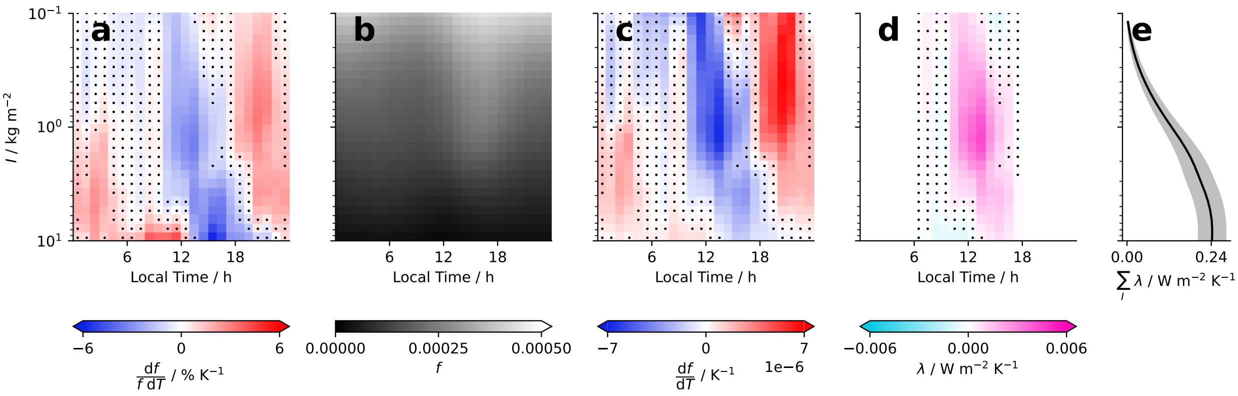

Fig. 5 (**a**) Relative change in the diurnal cycle of f in response to surface warming, (**b**) temporal mean of f, (**c**) absolute change in diurnal cycle of f in response to surface warming, (**d**) feedback λ from changes in the diurnal cycle of f and (**e**) cumulative sum of λ over I. Dots indicate trends statistically insignificant at a 95% confidence level, and the shaded area in **d** visualises the standard deviation derived from bootstrapping.

f and is defined as negative for increasing reflected radiation:

$$\lambda(l, I) = -\frac{\mathrm{d}R}{\mathrm{d}T}(l, I) = -S(l)\frac{\mathrm{d}f}{\mathrm{d}T}(l, I) \cdot \left[\alpha_{\mathrm{cl}}(l, I) - \alpha_{\mathrm{cs}}\right]. \tag{3}$$

We calculate $\alpha_{\mathrm{cl}}(l, I)$ and S from GSRM data (see Methods) and assume $\alpha_{\mathrm{cs}} = 0.1$. The change in the diurnal cycle of f with surface warming is derived from a linear regression of $f(l, I)$ against T in every (l, I) bin. Again, trends in $f(l, I)$ that are uniform across the day are excluded by normalising $f(l, I)$ for every timestep (see Methods). Since S is zero during the night, λ will also be zero at night.

Clouds of all considered thicknesses occur less during the day and more during the night in response to surface warming (Fig. 5a). This signal is statistically significant for all clouds and strongest for the thickest clouds. The absolute change in f is derived by multiplying the relative change in f (Fig. 5a) with the mean f (Fig. 5b). Since clouds become less frequent the thicker they are, the absolute change in f is small for thick clouds (Fig. 5c).

Clouds around $I = 1$ kg m^{-2} contribute most to the positive feedback from the diurnal cycle change of deep convection (Fig. 5d). Thicker clouds are too few to produce a substantial λ, and as clouds become thinner than $I = 1$ kg m^{-2} their albedo starts to decrease (Fig. S4), which limits their ability to contribute to λ. That the majority of λ stems from clouds around $I = 1$ kg m^{-2} also becomes visible in the cumulative sum of λ over I, which has the largest slope at $I = 1$ kg m^{-2}.

The diurnal-cycle feedback is positive and of the same order of magnitude as other cloud feedbacks. We derive $\lambda = 0.24 \pm 0.04$ W m^{-2} K^{-1}, with the error estimate being derived from bootstrapping (see Methods). This is higher than the first estimates of the diurnal-cycle feedback from GSRM aquaplanet simulations [22], which yield $\lambda = 0.2$ W m^{-2} K^{-1} for a 2 K surface warming and $\lambda = 0.1$ W m^{-2} K^{-1} for a 4 K surface warming. We scale our observational estimate of the diurnal-cycle feedback in the tropics to a global mean feedback by dividing the feedback value by two, since the tropics cover only half of the Earth's surface. The global mean diurnal-cycle feedback of $\lambda = 0.12 \pm 0.02$ W m^{-2} K^{-1} is of comparable magnitude to other cloud feedbacks, which range from 0.08 W m^{-2} K^{-1} to 0.25 W m^{-2} K^{-1} [2].

While internal variability within observations confirms the positive diurnal-cycle feedback found in idealised simulations, some questions remain open. It remains unclear whether the diurnal-cycle feedback diagnosed from internal variability is similar to the feedback acting on the long-term warming trend. Internal variability has been used before to assess the response of tropical high clouds to surface warming [36, 37] and to constrain high-cloud feedbacks [34], but the similarity of the high-cloud response to warming from internal variability and the long-term trend has not yet been tested. A second open question is how the diurnal cycle of deep convection is impacted by CO_2 radiative forcing. If the mechanism causing the reduction of daytime deep convection depends on cloud radiative heating as hypothesised in [16], it might be impacted by CO_2 directly.

6 Conclusion

The diurnal cycle of tropical deep convection changes in response to surface warming, with deep convection occurring less during the day and more during the night. We confirm this finding from GSRM aquaplanet simulations [16] by using the internal variability within satellite observations of ice water path. The response of the diurnal cycle of deep convection to surface warming is similar in the simulations and observations, but the magnitude of the response is about twice as large in the observations.

The change in the diurnal cycle of deep convection is remarkably similar over land and ocean, despite the mean diurnal cycle being much more pronounced over land. That daytime deep convection reduces similarly over land and ocean points towards a shared mechanism that is independent of the surface type. One proposed explanation is that a higher magnitude of cloud radiative heating in response to surface warming could alter the diurnal cycle of deep convection [16]. However, targeted mechanism-denial simulations are required to test this hypothesis.

The change in the diurnal cycle of clouds produced by deep convection results in a positive climate feedback that adds to previous assessments of the cloud feedback [1–6], implying a higher climate sensitivity. Deep convective clouds and thick anvils reduce during the day, causing more solar radiation to be absorbed by the surface, which amplifies surface warming. Previous studies targeting the feedback from tropical high clouds were not capturing this feedback because the diurnal cycle was averaged out in their analyses [4, 20, 34, 35].

This study is one example of why it is necessary and timely to take climate science beyond the analysis of the mean state [38]. It is timely because tools like machine learning and higher computational power enable datasets like CCIC [24, 25] and high-resolution simulations, which allow us to identify single deep convective cells and their diurnal cycle. It is necessary because otherwise important climate phenomena like the diurnal-cycle feedback would remain buried in the mean.

7 Methods

Our method is independent of whether I or T_b are used for identifying deep convective clouds. For simplicity, we only use I throughout the remainder of the methods section.

7.1 Histograms and Cloud Fraction

At the heart of our analysis are histograms of I with three dimensions: local time in hours (l), I in kg m^{-2} and time (t) in months. For every month, we count the number of occurrences (N) within every I and l bin from the original I data, which has a 30-minute timestep and 0.036° horizontal grid spacing. The 3D histograms are calculated for the entire tropics (30°S to 30°N), as well as for tropical ocean and land areas separately.

We derive cloud fractions (f) averaged over the respective region from the histograms by division:

$$f(t,l,I) = \frac{N(t,l,I)}{\sum_{l=0}^{24}\sum_{I=0}^{\infty} N(t,l,I)}. \tag{4}$$

f should be interpreted as the area fraction covered by clouds within the respective (l, I) bin for a given month. The fraction of deep convective clouds (f_d) with $I > 1$ kg m^{-2} for each local time is then calculated as

$$f_\mathrm{d}(t,l) = \sum_{I=1}^{\infty} f(t,l,I). \tag{5}$$

The total f_d is given by

$$f_\mathrm{d}(t) = \sum_{l=0}^{24} f_\mathrm{d}(t,l), \tag{6}$$

which should be interpreted as the cloud fraction with $I > 1$ kg m^{-2} in the given month.

We neglect the dependence of grid cell area on the latitude in our calculation of N and hence also f. The I data is on a regular latitude longitude grid, so the grid cell area will decrease with $\cos(\phi)$, where ϕ is latitude. For our calculation of $N(t,l,I)$, we simply count the number of occurrences within every bin, without accounting for the varying grid cell area by weighting with $cos(\phi)$. Implementing such an area weighting would complicate the calculation of $N(t,l,I)$ substantially. We regard this simplification as justified, since $\cos\phi$ only varies from 0.87 to 1 within 30°S to 30°N.

7.2 Regression

As the predictor for changes in f, we use the two-meter temperature (T) from ERA5 [33], which is area-weighted and averaged over the entire tropics, as well as over tropical land and tropical oceans separately. Since f has a monthly timestep, we use monthly means of T. The regression works the same for the 3D $f(t,l,I)$ and the 2D $f_{\mathrm{d}}(t,l)$. For simplicity, we only show equations for $f(t,l,I)$.

To isolate changes in the diurnal cycle of f from changes in f that are uniform across the diurnal cycle, we normalise cloud fractions with respect to local time, which we denote as $\bar{f}$:

$$\bar{f}(t,l,I) = \frac{f(t,l,I)}{\sum_{l=0}^{24} f(t,l,I)} \tag{7}$$

This ensures that $\sum_{l=0}^{24} \bar{f}_{I=x} = 1$ for every timestep, where $\bar{f}_{I=x}$ denotes the normalised cloud fraction at any I.

We detrend and deseasonalize $\bar{f}$ and T along the time dimension to isolate only El-Niño-driven internal variability (Fig. S5). To detrend the data, we subtract the linear trend over time. To deseasonalize the data, we subtract the mean annual cycle. The resulting timeseries of $\bar{f}$ and T are used to calculate their linear regression within every (l,I) bin. The slope (s) derived from the linear regression is used to calculate the relative change in the diurnal cycle of f as

$$\frac{\mathrm{d}f}{f\mathrm{d}T}(l,I) = \frac{s(l,I)}{\langle \bar{f}(t,l,I)\rangle} \cdot 100\%, \tag{8}$$

where $\langle\cdot\rangle$ denotes the temporal mean over the whole timeseries.

7.3 Feedback

We calculate the diurnal-cycle feedback (λ) from clouds with $I > 0.1$ kg m^{-2} with Eq. 3. The cloud albedo (α_{cl}) used in Eq. 3 is calculated from the radiative fluxes of the GSRM aquaplanet control simulation described in [16] using the method from [22]. That means α_{cl} is calculated from the all-sky albedo $\alpha_{\mathrm{as}} = R_{\mathrm{as}}/S$ with R_{as} being the reflected all-sky SW flux at the top of the atmosphere (TOA) and the clear-sky albedo $\alpha_{\mathrm{cs}} = R_{\mathrm{cs}}/S$ with R_{cs} being the reflected clear-sky SW flux at TOA:

$$\alpha_{\mathrm{cl}} = \frac{\alpha_{\mathrm{as}} - \alpha_{\mathrm{cs}}}{1 + \alpha_{\mathrm{cs}}(\alpha_{\mathrm{as}} - 2)}.$$

We bin α_{cl} by I and l to calculate the mean $\alpha_{\mathrm{cl}}(l,I)$ (Fig. S4).

The incoming solar radiation is also diagnosed from the aquaplanet GSRM simulations (Fig. S3). We use one day (2021-07-02) of the coupled ICON-C4 simulation described in [39] to calculate the upwelling longwave radiation in tropical clear-sky regions (Fig. S3). While this quantity is not necessary to calculate λ, we use it to argue why λ only acts in the shortwave spectrum (Sec. 5).

The total λ is calculated as

$$\lambda = \sum_{l=0}^{24} \sum_{I=0.1}^{\infty} \lambda(l,I). \tag{9}$$

7.4 Bootstrapping

We estimate the uncertainty in λ using block bootstrapping applied to the linear regression between f and T. To account for the autocorrelation in T, which persists for up to three years (Fig. S5), we randomly sample three-year segments from the time series. We draw eight blocks to closely match the length (n) of the bootstrap and original time series. The starting indices i_k, $k = 1, \ldots, 8$, are randomly drawn from $\{0, 1, \ldots, n-36\}$ without replacement. The bootstrapped time series are defined as

$$T_{\mathrm{bs}}(t) = \{T(t_{i_k}, \ldots, t_{i_k+36})\}, \tag{10}$$

$$f_{\mathrm{bs}}(t, l, I) = \{f(t_{i_k}, \ldots, t_{i_k+36}, l, I)\}. \quad (11)$$

The bootstrapped time series $T_{\mathrm{bs}}(t)$ and $f_{\mathrm{bs}}(t, l, I)$ are then used to recompute $\mathrm{d}f/f\mathrm{d}T(l, I)$ via linear regression (Eq. 8), from which λ is calculated using Eq. 3. We calculate the mean and standard deviation of λ from 2000 bootstrap samples, which is the sample size for which λ converges (Fig. S6).

Acknowledgements The authors thank Blaž Gasparini and James Ruppert for inspiring discussions.

Funding This research was funded by the Deutsche Forschungsgemeinschaft (DFG, German Research Foundation) under Germany's Excellence Strategy – EXC 2037 'CLICCS - Climate, Climatic Change, and Society' – Project Number: 390683824. This work used resources of the Deutsches Klimarechenzentrum (DKRZ) granted by its Scientific Steering Committee (WLA) under project ID bm1183.

Code Availability The code to reproduce the figures and numbers from this paper is available from https://doi.org/10.5281/zenodo.19245767 [40].

Data Availability The CCIC data was accessed on 2026-01-08 and is available from https://registry.opendata.aws/ccic. The brightness temperature data was accessed on 2025-11-19 and is available from https://disc.gsfc.nasa.gov/datasets/GPM_MERGIR_1/summary. The data to reproduce the figures and numbers from this paper is available from https://doi.org/10.5281/zenodo.19245784 [41].

Author Contribution All authors contributed to designing the research. J.D. carried out the research and wrote the paper with input from all co-authors. J.W. designed the schematic (Fig. 4).

References

[1] Arias, P.A., Bellouin, N., Coppola, E., Jones, R.G., Krinner, G., Marotzke, J., Naik, V., Palmer, M.D., Plattner, G.-K., Rogelj, J., Rojas, M., Sillmann, J., Storelvmo, T., Thorne, P.W., Trewin, B., Achuta Rao, K., Adhikary, B., Allan, R.P., Armour, K., Bala, G., Barimalala, R., Berger, S., Canadell, J.G., Cassou, C., Cherchi, A., Collins, W., Collins, W.D., Connors, S.L., Corti, S., Cruz, F., Dentener, F.J., Dereczynski, C., Di Luca, A., Diongue Niang, A., Doblas-Reyes, F.J., Dosio, A., Douville, H., Engelbrecht, F., Eyring, V., Fischer, E., Forster, P., Fox-Kemper, B., Fuglestvedt, J.S., Fyfe, J.C., Gillett, N.P., Goldfarb, L., Gorodetskaya, I., Gutierrez, J.M., Hamdi, R., Hawkins, E., Hewitt, H.T., Hope, P., Islam, A.S., Jones, C., Kaufman, D.S., Kopp, R.E., Kosaka, Y., Kossin, J., Krakovska, S., Lee, J.-Y., Li, J., Mauritsen, T., Maycock, T.K., Meinshausen, M., Min, S.-K., Monteiro, P.M.S., Ngo-Duc, T., Otto, F., Pinto, I., Pirani, A., Raghavan, K., Ranasinghe, R., Ruane, A.C., Ruiz, L., Sallée, J.-B., Samset, B.H., Sathyendranath, S., Seneviratne, S.I., Sörensson, A.A., Szopa, S., Takayabu, I., Treguier, A.-M., Hurk, B., Vautard, R., Schuckmann, K., Zaehle, S., Zhang, X., Zickfeld, K.: Technical summary. In: Masson-Delmotte, V., Zhai, P., Pirani, A., Connors, S.L., Péan, C., Berger, S., Caud, N., Chen, Y., Goldfarb, L., Gomis, M.I., Huang, M., Leitzell, K., Lonnoy, E., Matthews, J.B.R., Maycock, T.K., Waterfield, T., Yelekçi, O., Yu, R., Zhou, B. (eds.) Climate Change 2021: The Physical Science Basis. Contribution of Working Group I to the Sixth Assessment Report of the Intergovernmental Panel on Climate Change, pp. 33–144. Cambridge University Press, Cambridge, UK and New York, NY, USA (2021). https://doi.org/10.1017/9781009157896.002

[2] Sherwood, S.C., Webb, M.J., Annan, J.D., Armour, K.C., Forster, P.M., Hargreaves, J.C., Hegerl, G., Klein, S.A., Marvel, K.D., Rohling, E.J., Watanabe, M., Andrews, T., Braconnot, P., Bretherton, C.S., Foster, G.L., Hausfather, Z., Heydt, A.S., Knutti, R., Mauritsen, T., Norris, J.R., Proistosescu, C., Rugenstein, M., Schmidt, G.A., Tokarska, K.B., Zelinka, M.D.: An Assessment of Earth's Climate Sensitivity Using Multiple Lines of Evidence. Reviews of Geophysics **58**(4), 2019–000678 (2020) https://doi.org/10.1029/2019RG000678 . _eprint: https://onlinelibrary.wiley.com/doi/pdf/10.1029/2019RG000678. Accessed 2023-06-05

[3] Ceppi, P., Brient, F., Zelinka, M.D., Hartmann, D.L.: Cloud feedback mechanisms and their representation in global climate models. WIREs Climate Change **8**(4), 465 (2017) https://doi.org/10.1002/wcc.465 . _eprint: https://wires.onlinelibrary.wiley.com/doi/pdf/10.1002/wcc.465. Accessed 2025-07-01

[4] Raghuraman, S.P., Medeiros, B., Gettelman, A.: Observational Quantification of Tropical High Cloud Changes and Feedbacks. Journal of Geophysical Research: Atmospheres **129**(7), 2023–039364 (2024) https://doi.org/10.1029/2023JD039364 . _eprint: https://onlinelibrary.wiley.com/doi/pdf/10.1029/2023JD039364. Accessed 2025-05-22

[5] Zelinka, M.D., Zhou, C., Klein, S.A.: Insights from a refined decomposition of cloud feedbacks. Geophysical Research Letters **43**(17), 9259–9269 (2016) https://doi.org/10.1002/2016GL069917 . _eprint: https://onlinelibrary.wiley.com/doi/pdf/10.1002/2016GL069917. Accessed 2023-06-01

[6] Zelinka, M.D., Klein, S.A., Qin, Y., Myers, T.A.: Evaluating Climate Models' Cloud Feedbacks Against Expert Judgment. Journal of Geophysical Research: Atmospheres **127**(2), 2021–035198 (2022) https://doi.org/10.1029/2021JD035198 . _eprint: https://onlinelibrary.wiley.com/doi/pdf/10.1029/2021JD035198. Accessed 2024-07-12

[7] Chen, T., Ge, J., Zhang, C., Wu, Y., Mu, Q., Han, X., Su, J., Hu, X., Zhu, Z.: Shifts in diurnal cycles of low and high clouds warm the climate: evidence from decadal satellite observations. Environmental Research Letters **20**(9), 094040 (2025) https://doi.org/10.1088/1748-9326/adf23c . Accessed 2026-03-10

[8] Luo, H., Quaas, J., Han, Y.: Diurnally asymmetric cloud cover trends amplify greenhouse warming. Science Advances **10**(25), 5179 (2024) https://doi.org/10.1126/sciadv.ado5179 . Accessed 2026-03-11

[9] Zelinka, M.D., Klein, S.A., Hartmann, D.L.: Computing and Partitioning Cloud Feedbacks Using Cloud Property Histograms. Part II: Attribution to Changes in Cloud Amount, Altitude, and Optical Depth (2012) https://doi.org/10.1175/JCLI-D-11-00249.1 . Section: Journal of Climate. Accessed 2025-06-10

[10] Zelinka, M.D., Klein, S.A., Hartmann, D.L.: Computing and Partitioning Cloud Feedbacks Using Cloud Property Histograms. Part I: Cloud Radiative Kernels (2012) https://doi.org/10.1175/JCLI-D-11-00248.1 . Chap. Journal of Climate. Accessed 2026-03-10

[11] Christopoulos, C., Schneider, T.: Assessing Biases and Climate Implications of the Diurnal Precipitation Cycle in Climate Models. Geophysical Research Letters **48**(13), 2021–093017 (2021) https://doi.org/10.1029/2021GL093017 . _eprint: https://agupubs.onlinelibrary.wiley.com/doi/pdf/10.1029/2021GL093017. Accessed 2026-01-26

[12] Covey, C., Gleckler, P.J., Doutriaux, C., Williams, D.N., Dai, A., Fasullo, J., Trenberth, K., Berg, A.: Metrics for the Diurnal Cycle of Precipitation: Toward Routine Benchmarks for Climate Models. Journal of Climate **29**(12), 4461–4471 (2016) https://doi.org/10.1175/JCLI-D-15-0664.1 . Chap. Journal of Climate. Accessed 2026-01-26

[13] Stevens, B., Acquistapace, C., Hansen, A., Heinze, R., Klinger, C., Klocke, D., Rybka, H., Schubotz, W., Windmiller, J., Adamidis, P., Arka, I., Barlakas, V., Biercamp, J., Brueck, M., Brune, S., Buehler, S.A., Burkhardt, U., Cioni, G., Costa-Surós, M., Crewell, S., Crüger, T., Deneke, H., Friederichs, P., Henken, C.C., Hohenegger, C., Jacob, M., Jakub, F., Kalthoff, N., Köhler, M., LAAR, T.W., Li, P., Löhnert, U., Macke, A., Madenach, N., Mayer, B., Nam, C., Naumann, A.K., Peters, K., Poll, S., Quaas, J., Röber, N., Rochetin, N., Scheck, L., Schemann, V., Schnitt, S., Seifert, A., Senf, F., Shapkalijevski, M., Simmer, C., Singh, S., Sourdeval, O., Spickermann, D., Strandgren, J., Tessiot, O., Vercauteren, N., Vial, J., Voigt, A., Zängl, G.: The Added Value of Large-eddy and Storm-resolving Models for Simulating Clouds and Precipitation. Journal of the Meteorological Society of Japan. Ser. II **98**(2), 395–435 (2020) https://doi.org/10.2151/jmsj.2020-021

[14] Song, J., Song, F., Feng, Z., Leung, L.R., Li, C., Wu, L.: Realistic Precipitation Diurnal Cycle in Global Convection-Permitting Models by Resolving Mesoscale Convective Systems. Geophysical Research Letters **51**(13), 2024–109945 (2024) https://doi.org/10.1029/2024GL109945 . _eprint: https://agupubs.onlinelibrary.wiley.com/doi/pdf/10.1029/2024GL109945. Accessed 2025-06-23

[15] Eriksson, P., Baró Pérez, A., Müller, N., Hallborn, H., May, E., Brath, M., Buehler, S.A., Ickes, L.: Advancements and continued challenges in observations and global modelling of atmospheric ice mass. Atmospheric Chemistry and Physics **26**(4), 2741–2768 (2026) https://doi.org/10.5194/acp-26-2741-2026

. Accessed 2026-03-09

[16] Deutloff, J., Buehler, S., Windmiller, J., Naumann, A.K.: Facets of the Tropical High-Cloud Feedback in a Global Storm-Resolving Model. Research Square. ISSN: 2693-5015 (2026). https://doi.org/10.21203/rs.3.rs-9133974/v1 . https://www.researchsquare.com/article/rs-9133974/v1 Accessed 2026-04-01

[17] Ruppert, J.H., Hohenegger, C.: Diurnal Circulation Adjustment and Organized Deep Convection. Journal of Climate (2018) https://doi.org/10.1175/JCLI-D-17-0693.1 . Section: Journal of Climate. Accessed 2025-08-27

[18] Gray, W.M., Jacobson, R.W.: Diurnal Variation of Deep Cumulus Convection. Monthly Weather Reviews (1977). Section: Monthly Weather Review. Accessed 2025-08-27

[19] Yang, S., Smith, E.A.: Mechanisms for Diurnal Variability of Global Tropical Rainfall Observed from TRMM. Journal of Climate (2006) https://doi.org/10.1175/JCLI3883.1 . Section: Journal of Climate. Accessed 2025-08-27

[20] Sokol, A.B., Wall, C.J., Hartmann, D.L.: Greater climate sensitivity implied by anvil cloud thinning. Nature Geoscience, 1–6 (2024) https://doi.org/10.1038/s41561-024-01420-6 . Publisher: Nature Publishing Group. Accessed 2024-04-29

[21] Gasparini, B., Blossey, P.N., Hartmann, D.L., Lin, G., Fan, J.: What Drives the Life Cycle of Tropical Anvil Clouds? Journal of Advances in Modeling Earth Systems **11**(8), 2586–2605 (2019) https://doi.org/10.1029/2019MS001736 . _eprint: https://onlinelibrary.wiley.com/doi/pdf/10.1029/2019MS001736. Accessed 2023-11-17

[22] Deutloff, J., Buehler, S.A., Brath, M., Naumann, A.K.: Insights on Tropical High-Cloud Radiative Effect From a New Conceptual Model. Journal of Advances in Modeling Earth Systems **17**(2), 2024–004615 (2025) https://doi.org/10.1029/2024MS004615 . _eprint: https://onlinelibrary.wiley.com/doi/pdf/10.1029/2024MS004615. Accessed 2025-03-03

[23] Bolot, M., Harris, L.M., Cheng, K.-Y., Merlis, T.M., Blossey, P.N., Bretherton, C.S., Clark, S.K., Kaltenbaugh, A., Zhou, L., Fueglistaler, S.: Kilometer-scale global warming simulations and active sensors reveal changes in tropical deep convection. npj Climate and Atmospheric Science **6**(1), 1–8 (2023) https://doi.org/10.1038/s41612-023-00525-w . Number: 1 Publisher: Nature Publishing Group. Accessed 2024-02-05

[24] Amell, A., Pfreundschuh, S., Eriksson, P.: The Chalmers Cloud Ice Climatology: retrieval implementation and validation. Atmospheric Measurement Techniques **17**(14), 4337–4368 (2024) https://doi.org/10.5194/amt-17-4337-2024 . Accessed 2024-10-12

[25] Pfreundschuh, S., Kukulies, J., Amell, A., Hallborn, H., May, E., Eriksson, P.: The Chalmers Cloud Ice Climatology: A Novel Robust Climate Record of Frozen Cloud Hydrometeor Concentrations. Journal of Geophysical Research: Atmospheres **130**(6), 2024–042618 (2025) https://doi.org/10.1029/2024JD042618 . _eprint: https://onlinelibrary.wiley.com/doi/pdf/10.1029/2024JD042618. Accessed 2025-05-20

[26] Deng, M., Mace, G.G., Wang, Z., Okamoto, H.: Tropical Composition, Cloud and Climate Coupling Experiment validation for cirrus cloud profiling retrieval using CloudSat radar and CALIPSO lidar. Journal of Geophysical Research: Atmospheres **115**(D10) (2010) https://doi.org/10.1029/2009JD013104 . _eprint: https://agupubs.onlinelibrary.wiley.com/doi/pdf/10.1029/2009JD013104. Accessed 2025-08-07

[27] Delanoë, J., Hogan, R.J.: Combined CloudSat-CALIPSO-MODIS retrievals of the properties of ice clouds. Journal of Geophysical Research: Atmospheres **115**(D4) (2010) https://doi.org/10.1029/2009JD012346 . _eprint: https://agupubs.onlinelibrary.wiley.com/doi/pdf/10.1029/2009JD012346. Accessed 2025-08-07

[28] Janowiak, J.E., Joyce, R.J., Yarosh, Y.: A Real-Time Global Half-Hourly Pixel-Resolution Infrared Dataset and Its Applications. Bulletin of the American Meteorological Society **82**(2), 205–218 (2001) https://doi.org/10.1175/1520-0477(2001)082⟨0205:ARTGHH⟩2.3.CO;2 . Chap. Bulletin of the American Meteorological Society. Accessed 2026-01-27

[29] Janowiak, J., Joyce, B., Xie, P.: NCEP/CPC L3 Half Hourly 4km Global (60S–60N) Merged IR V1. Goddard Earth Sciences Data and Information Services Center (GES DISC), Greenbelt, MD. Accessed: 2026-01-27 (2017). https://doi.org/10.5067/P4HZB9N27EKU

[30] Hendon, H.H., Woodberry, K.: The diurnal cycle of tropical convection. Journal of Geophysical Research: Atmospheres **98**(D9), 16623–16637 (1993) https://doi.org/10.1029/93JD00525 . _eprint: https://agupubs.onlinelibrary.wiley.com/doi/pdf/10.1029/93JD00525. Accessed 2026-03-23

[31] Yang, G.-Y., Slingo, J.: The Diurnal Cycle in the Tropics. Monthly Weather Review **129**(4), 784–801 (2001) https://doi.org/10.1175/1520-0493(2001)129⟨0784:TDCITT⟩2.0.CO;2 . Chap. Monthly Weather Review. Accessed 2026-01-27

[32] Duvel, J.P.: Convection over Tropical Africa and the Atlantic Ocean during Northern Summer. Part I: Interannual and Diurnal Variations. Monthly Weather Review **117**(12), 2782–2799 (1989) https://doi.org/10.1175/1520-0493(1989)117⟨2782:COTAAT⟩2.0.CO;2 . Chap. Monthly Weather Review. Accessed 2026-01-27

[33] Hersbach, H., Bell, B., Berrisford, P., Hirahara, S., Horányi, A., Muñoz-Sabater, J., Nicolas, J., Peubey, C., Radu, R., Schepers, D., Simmons, A., Soci, C., Abdalla, S., Abellan, X., Balsamo, G., Bechtold, P., Biavati, G., Bidlot, J., Bonavita, M., De Chiara, G., Dahlgren, P., Dee, D., Diamantakis, M., Dragani, R., Flemming, J., Forbes, R., Fuentes, M., Geer, A., Haimberger, L., Healy, S., Hogan, R.J., Hólm, E., Janisková, M., Keeley, S., Laloyaux, P., Lopez, P., Lupu, C., Radnoti, G., Rosnay, P., Rozum, I., Vamborg, F., Villaume, S., Thépaut, J.-N.: The ERA5 global reanalysis. Quarterly Journal of the Royal Meteorological Society **146**(730), 1999–2049 (2020) https://doi.org/10.1002/qj.3803 . _eprint: https://rmets.onlinelibrary.wiley.com/doi/pdf/10.1002/qj.3803. Accessed 2026-01-19

[34] McKim, B., Bony, S., Dufresne, J.-L.: Weak anvil cloud area feedback suggested by physical and observational constraints. Nature Geoscience, 1–6 (2024) https://doi.org/10.1038/s41561-024-01414-4 . Publisher: Nature Publishing Group. Accessed 2024-04-29

[35] Wilson Kemsley, S., Nowack, P., Ceppi, P.: Climate Models Underestimate Global Decreases in High-Cloud Amount With Warming. Geophysical Research Letters **52**(7), 2024–113316 (2025) https://doi.org/10.1029/2024GL113316 . _eprint: https://onlinelibrary.wiley.com/doi/pdf/10.1029/2024GL113316. Accessed 2025-05-22

[36] Zelinka, M.D., Hartmann, D.L.: The observed sensitivity of high clouds to mean surface temperature anomalies in the tropics: TEMPERATURE SENSITIVITY OF HIGH CLOUDS. Journal of Geophysical Research: Atmospheres **116**(D23), (2011) https://doi.org/10.1029/2011JD016459 . Accessed 2025-07-01

[37] Saint-Lu, M., Bony, S., Dufresne, J.-L.: Clear-sky control of anvils in response to increased CO2 or surface warming or volcanic eruptions. npj Climate and Atmospheric Science **5**(1), 1–8 (2022) https://doi.org/10.1038/s41612-022-00304-z . Number: 1 Publisher: Nature Publishing Group. Accessed 2023-06-19

[38] Shaw, T.A., Stevens, B.: The other climate crisis. Nature **639**(8056), 877–887 (2025) https://doi.org/10.1038/s41586-025-08680-1 . Accessed 2025-03-31

[39] Segura, H., Pedruzo-Bagazgoitia, X., Weiss, P., Müller, S.K., Rackow, T., Lee, J., Dolores-Tesillos, E., Benedict, I., Aengenheyster, M., Aguridan, R., Arduini, G., Baker, A.J., Bao, J., Bastin, S., Baulenas, E., Becker, T., Beyer, S., Bockelmann, H., Brüggemann, N., Brunner, L., Cheedela, S.K., Das, S., Denissen, J., Dragaud, I., Dziekan, P., Ekblom, M., Engels, J.F., Esch, M., Forbes, R., Frauen, C., Freischem, L., García-Maroto, D., Geier, P., Gierz, P., González-Cervera, A., Grayson, K., Griffith, M., Gutjahr, O., Haak, H., Hadade, I., Haslehner, K., Hasson, S., Hegewald, J., Kluft, L., Koldunov, A., Koldunov, N., Kölling, T., Koseki, S., Kosukhin, S., Kousal, J., Kuma, P., Kumar, A.U., Li, R.,

Maury, N., Meindl, M., Milinski, S., Mogensen, K., Niraula, B., Nowak, J., Praturi, D.S., Proske, U., Putrasahan, D., Redler, R., Santuy, D., Sármány, D., Schnur, R., Scholz, P., Sidorenko, D., Spät, D., Sützl, B., Takasuka, D., Tompkins, A., Uribe, A., Valentini, M., Veerman, M., Voigt, A., Warnau, S., Wachsmann, F., Wacławczyk, M., Wedi, N., Wieners, K.-H., Wille, J., Winkler, M., Wu, Y., Ziemen, F., Zimmermann, J., Bender, F.A.-M., Bojovic, D., Bony, S., Bordoni, S., Brehmer, P., Dengler, M., Dutra, E., Faye, S., Fischer, E., Heerwaarden, C., Hohenegger, C., Järvinen, H., Jochum, M., Jung, T., Jungclaus, J.H., Keenlyside, N.S., Klocke, D., Konow, H., Klose, M., Malinowski, S., Martius, O., Mauritsen, T., Mellado, J.P., Mieslinger, T., Mohino, E., Pawłowska, H., Peters-von Gehlen, K., Sarré, A., Sobhani, P., Stier, P., Tuppi, L., Vidale, P.L., Sandu, I., Stevens, B.: nextGEMS: entering the era of kilometer-scale Earth system modeling. Geoscientific Model Development **18**(20), 7735–7761 (2025) https://doi.org/10.5194/gmd-18-7735-2025 . Accessed 2026-03-12

[40] Deutloff, J.: Code to accompany "Observed Diurnal Cycle Change of Tropical Deep Convection Amplifies Surface Warming" by Deutloff et al., 2026. Zenodo (2026). https://doi.org/10.5281/zenodo.19245767

[41] Deutloff, J.: Data to accompany "Observed Diurnal Cycle Change of Tropical Deep Convection Amplifies Surface Warming" by Deutloff et al., 2026. Zenodo (2026). https://doi.org/10.5281/zenodo.19245784

Supplementary Files

This is a list of supplementary files associated with this preprint. Click to download.

- supplement.pdf